Oligomerization of the Amide Sensor Protein AmiC by X-ray and Neutron Scattering and Molecular Modeling

Dean Chamberlain,[‡] Bernard P. O'Hara,[§] Stuart A. Wilson,[§,||] Laurence H. Pearl,[§] and Stephen J. Perkins*,[‡]

Department of Biochemistry and Molecular Biology, Royal Free Hospital School of Medicine, Rowland Hill Street, London NW3 2PF, U.K., and Department of Biochemistry and Molecular Biology, University College London, Gower Street, London WC1E 6BT, U.K.

Received February 12, 1997; Revised Manuscript Received April 22, 1997[⊗]

ABSTRACT: AmiC is the negative regulator of the amidase operon which is involved in amide metabolism in the cytosol of *Pseudomonas aeruginosa*. Crystal structures show that AmiC contains two large domains that are very similar to the periplasmic leucine−isoleucine−valine binding protein (LivJ) of *Escherichia coli*. Synchrotron X-ray and neutron (in 100% ^2H_2O buffer) scattering data were obtained for AmiC in the presence of its substrate acetamide and its anti-inducer butyramide which binds more weakly to AmiC than acetamide. Guinier analyses to obtain radius of gyration R_G and molecular weight M_r values showed that AmiC formed trimers whose formation was favored in the presence of acetamide and which exhibited concentration-dependent properties at concentrations between 0.4 and 2 mg/mL. Above 2 mg/mL, where trimers predominated, the R_G data were identical within 0.05 nm for AmiC−acetamide and AmiC−butyramide with mean X-ray and neutron R_G values of 3.35 and 3.28 nm, respectively. Scattering curve fits constrained by the crystal structure of AmiC−acetamide were evaluated in order to describe a model for trimeric AmiC. A translational search of parallel alignments of three monomers to form a symmetric AmiC homotrimer gave a good X-ray curve fit. Combinations of calculated curves for monomeric, dimeric, trimeric, and tetrameric AmiC as seen in the crystal structure of AmiC gave reasonable but weaker X-ray curve fits which did not favor the existence of tetrameric AmiC. It is concluded that AmiC exhibits novel ligand-dependent oligomerization properties in solution when these are compared to other members of the periplasmic binding protein superfamily, where AmiC exists in monomeric and trimeric forms, the proportions of which depend on the presence of acetamide or butyramide.

Pseudomonas aeruginosa is a ubiquitous gram negative rod-shaped bacterium that is an important opportunistic pathogen in man and other animals (Singleton & Sainsbury, 1987; Jawetz et al., 1987; Koch & Høiby, 1992). It can be isolated from infected burns, urinary tract infections, and the lungs of patients with cystic fibrosis. It can occasionally be pathogenic in stressed plants. *P. aeruginosa* can utilize short-chain aliphatic amides such as acetamide $CH_3{\cdot}CO{\cdot}NH_2$ as sole carbon and nitrogen sources, and these are hydrolyzed to ammonia and acetic acid. The enzyme system is induced by the presence of amides (Kelly & Clarke, 1962; Stanier et al., 1966). The amidase operon consists of five genes, namely, *amiE, amiB, amiC, amiR,* and *amiS,* in that order. AmiC is a soluble cytoplasmic protein that functions as an amide sensor and negative regulator of the amidase operon. AmiC controls the activity of the transcription antitermination factor AmiR, which in turn regulates expression of the amidase enzyme system. *amiE* is the gene which corresponds to the amidase enzyme, and *amiB* and *amiS* appear to form a membrane transport system for the importation of amide into the bacteria (Drew & Wilson, 1992; Wilson et al., 1995).

The combination of secondary structure predictions and fold recognition analyses indicated that, despite only 17% amino acid sequence identity, AmiC had the same protein fold as the leucine−isoleucine−valine binding protein (LivJ) of *Escherichia coli* (Sack et al., 1989a; Wilson et al., 1993). LivJ corresponds to the Cluster 4 subclass of periplasmic binding proteins (Tam & Saier, 1993). The prediction was confirmed by the crystal structure of AmiC bound to its substrate acetamide (Pearl et al., 1994). The similarity of the AmiC structure to that of periplasmic binding proteins is of interest in that these proteins form a large family of related structures that are involved with the transport of small molecules into bacteria (Tam & Saier, 1993). A total of eight different prokaryotic subclasses that bind to sugars, amino acids, and anions have been identified, and crystal structures have been determined for six of these (Table 1). Nonetheless AmiC exhibits distinct functional properties in that it controls AmiR in response to a signal from acetamide, while the periplasmic binding proteins transport small molecules within the inner bacterial membrane. A similar relationship with LivJ has also been identified for the extracellular domain of the eukaryotic protein glutamate receptor, which is involved in neurotransmitter activity (O'Hara et al., 1993; Stern-Bach et al., 1994). AmiC is constructed from two nonequivalent α-helix/β-sheet domains joined by three polypeptide links which flank a ligand-binding site in a large cleft between them (Figure 1). Interestingly, the binding site cleft in LivJ is opened by a domain movement of approximately 35° compared to that in AmiC (Figure 1). In the AmiC−acetamide crystal

* To whom correspondence and requests for reprints should be addressed.
[‡] Royal Free Hospital School of Medicine.
[§] University College London.
[||] Present address: Department of Biochemistry, University of Oxford, South Parks Road, Oxford OX1 3QU, U.K.
[⊗] Abstract published in *Advance ACS Abstracts,* June 15, 1997.

S0006-2960(97)00325-5 CCC: $14.00

Table 1: R_G Analyses of Representative Crystal Structures for Periplasmic Binding Proteins[a]

periplasmic binding protein	Brookhaven PDB code	R_G (nm)	reference
Cluster 1 (molecular weight 40 600)			
maltodextrin-binding protein	1omp	2.48	Sharff et al. (1992)
maltodextrin-binding protein + maltose	2mbp	2.39	Spurlino et al. (1991)
Cluster 2 (molecular weight 33 000)			
arabinose binding protein + ligand	1abe, 1abf, 5abp	2.24−2.26	Quiocho et al. (1989)
Cluster 3 (molecular weight 26 100)			
histidine-binding protein + histidine	1hpb, 1hsl	1.99−2.02	Oh et al. (1994); Yao et al. (1994)
Lys−Arg−Orn-binding protein	2lao	2.12	Oh et al. (1993)
Lys−Arg−Orn-binding protein + ligand	1lst, 1laf, 1lah, 1lag	1.99	Oh et al. (1993)
Cluster 4 (molecular weight 36 800 and 41 200)			
Leu−Ile−Val-binding protein LivJ	2liv	2.43	Sack et al. (1989a)
leucine-binding protein	2lbp	2.44	Sack et al. (1989b)
acetamide-binding protein AmiC + acetamide	1pea	2.23	Pearl et al. (1994)
acetamide-binding protein AmiC + butyramide	-	2.25	O'Hara et al. (1997)
Cluster 5 (molecular weight 59 100)			
oligopeptide-binding protein + tri-/tetrapeptide	1ola, 1olb	2.54−2.56	Tame et al. (1994)
Cluster 6 (molecular weight 34 300)			
phosphate-binding protein + phosphate	1abh	2.23	Luecke & Quiocho (1990)
sulfate-binding protein + sulfate	1sbp	2.15	Pflugrath & Quiocho (1988)

[a] Crystal structures for at least 35 periplasmic binding proteins are available in the Brookhaven database.

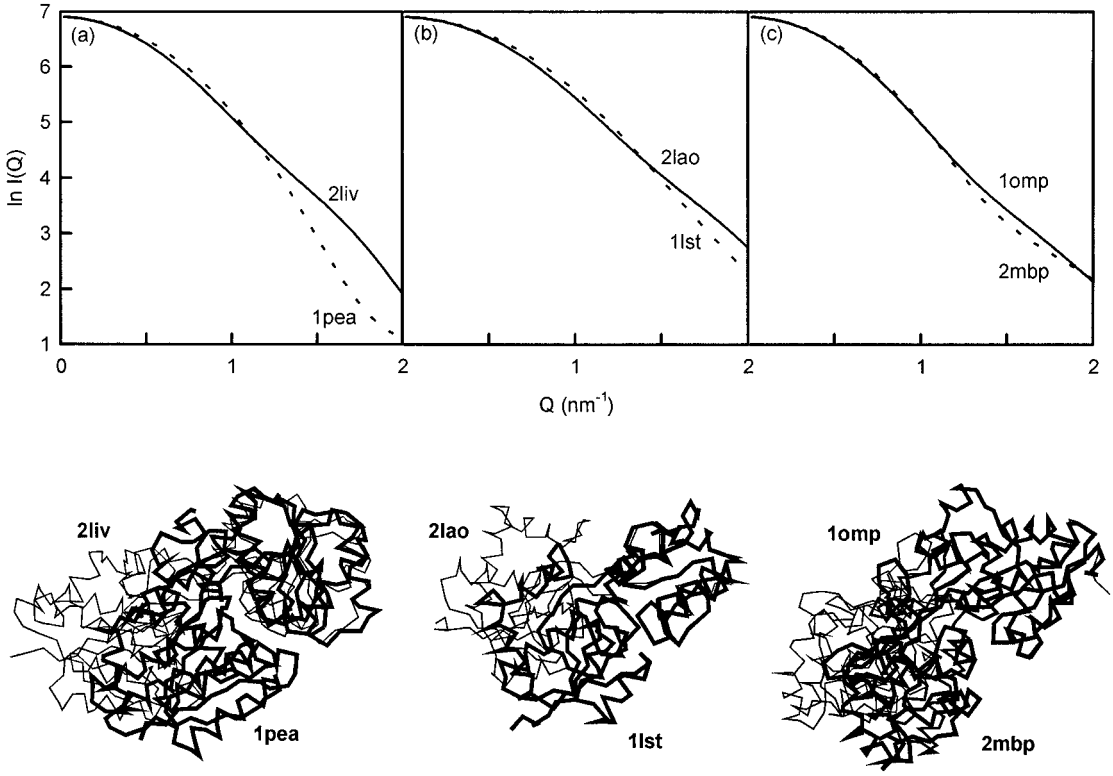

FIGURE 1: X-ray scattering curve simulations for Clusters 4, 3, and 1 of the periplasmic binding proteins. The dashed scattering curves correspond to the closed conformations. The α-carbon coordinates of the two proteins are shown with the C-terminal domains superimposed, and the closed conformations are represented in bold outline. The views of the α-carbon traces are shown to maximise the domain movement seen between the open and closed forms. (a) AmiC (1pea) and LivJ (2liv) in Cluster 4 were represented by 623 and 559 spheres, respectively, of radius 0.220 nm. (b) Lysine−argine−ornithine-binding protein (1lst and 2lao) in Cluster 3 was represented by 398 spheres of radius 0.220 nm. (c) Maltodextrin-binding protein (1omp and 2mbp) in Cluster 1 were represented by 94 and 96 spheres, respectively, of radius 0.410 and 0.405 nm.

structure, the cleft is substantially closed. The AmiC amide binding site is extremely specific for acetamide with a dissociation constant of 3.7 μM. Butyramide $CH_3{\cdot}CH_2{\cdot}CH_2{\cdot}CO{\cdot}NH_2$ is an anti-inducer of AmiC and has a 100-fold larger dissociation constant. It is possible that AmiC−acetamide and AmiC−butyramide may possess alternative conformations.

Small-angle X-ray and neutron scattering are powerful low-resolution methods for studies of the arrangement of domains in multidomain proteins and their degree of oligomerization (Perkins, 1988). They have advantages in that the data are obtained in solution. The utility of the methods has been much improved by the development of calibrated procedures for the calculation of scattering curves from known crystal structures (Smith et al., 1990; Perkins et al., 1993). Automated scattering curve fit procedures constrained by known atomic structures can now be used to assess the unknown structure of a multidomain protein (Mayans et al., 1995; Beavil et al., 1995; Boehm et al., 1996). The previous application of X-ray scattering to periplasmic binding

proteins showed that L-arabinose binding protein was monomeric, and that on the addition of L-arabinose its R_G value of 2.12 nm decreased by 0.094 ± 0.033 nm (Newcomer et al., 1981). This decrease corresponded to a rotation of the two domains closer to one another by 18° ± 4°. Other periplasmic binding proteins showed a 52° domain rotation between ligated and unligated lysine−arginine−ornithine binding protein (Oh et al., 1993), and a 35° domain rotation between ligated and unligated maltodextrin binding protein (Sharff et al., 1992) (Figure 1). Here, X-ray and neutron scattering methods are applied to determine the solution structure of AmiC. Unlike the classical periplasmic binding proteins which are monomeric, we show that AmiC exists in monomeric and trimeric forms, the proportions of which depend on the presence of acetamide or butyramide. We assess whether a ligand-dependent conformational change may occur and describe how automated curve fit methods can be applied to interpret the scattering curves in terms of a structure for trimeric AmiC.

MATERIALS AND METHODS

(a) Expression and Purification of AmiC for Solution Scattering

The expression system consisted of a 1.3×10^3 base pair fragment of the amidase system containing the *amiC* open reading frame, cloned into a broad host range vector pMMB66HE, and transformed into a *P. aeruginosa* amidase deletion strain as described and characterized by Wilson and Drew (1991). The bacteria were fermented in a modified Oxoid No. 2 broth, and protein expression was started by the addition of isopropyl β-D-thiogalactopyranoside. Cells were harvested by low-speed centrifugation and lysed immediately by sonication in AmiC buffer (20 mM Tris-HCl, pH 8.0, 1 mM dithiothreitol, 1 mM EDTA, 1 mM phenylmethylsulfonyl fluoride) (Wilson et al., 1991). The supernatant after sonication was clarified by centrifugation at 25000*g* for 30 min, and AmiC was precipitated using 40−60% saturated $(NH_4)_2SO_4$. The AmiC fractions were pooled, resuspended in AmiC buffer and dialyzed overnight to remove $(NH_4)_2SO_4$. AmiC was purified further by ion exchange (Q-Sepharose, Pharmacia) when it was eluted in the range 450−550 mM NaCl using a 0−1 M NaCl gradient. These fractions were pooled, made up to 1.2 M $(NH_4)_2SO_4$, loaded onto a phenyl-Sepharose hydrophobic interaction column, and eluted using a 0−1 M $(NH_4)_2SO_4$ gradient. The pooled AmiC fractions were dialyzed for several days against AmiC buffer containing 10 mM butyramide to remove acetamide. AmiC was then concentrated in an Amicon pressure cell and purified by gel filtration as a single peak to give concentrations of up to 17 mg/mL. The absorption coefficient of AmiC (1%, 1 cm, 280 nm) was calculated as 13.6 (Perkins, 1986).

AmiC samples were stored at 4 °C and used within a few days for scattering experiments. For X-ray scattering and neutron scattering in H_2O buffers, the AmiC−butyramide samples were used as prepared above, and AmiC−acetamide was generated by adding 10 mM acetamide immediately prior to data collection to displace butyramide. For neutron scattering in ^2H_2O buffers, the AmiC−butyramide samples were dialyzed for 36 h with four buffer changes into AmiC buffer prepared in ^2H_2O and containing either 10 mM acetamide or butyramide. Alternatively, AmiC−butyramide was dialyzed into its ^2H_2O buffer containing 10 mM butyramide, and AmiC−acetamide was generated by adding 10 mM-acetamide in AmiC buffer in ^2H_2O immediately prior to data collection.

(b) X-ray and Neutron Scattering Data Collection

X-ray scattering curves were obtained in two beam sessions using a camera with a quadrant detector at Station 2.1 at the Synchrotron Radiation Source, Daresbury, U.K. (Towns-Andrews et al., 1989; Worgan et al., 1990). Sample−detector distances of 3.14 or 3.17 m were used, with beam currents of 122−173 mA and a storage ring energy of 2.0 GeV. This resulted in a usable Q range of 0.1−2.3 nm^{-1} ($Q = 4\pi \sin\theta/\lambda$; scattering angle $= 2\theta$; wavelength $= \lambda$). Data acquisition times were 10 min, obtained as 10 time frames of 1 min each as a control for radiation damage. Other details of data collection and analyses are described elsewhere [e.g., Beavil et al. (1995)]. Sample temperatures were set at 15 °C.

Neutron scattering data were obtained in one session on Instrument D11 at the Institut Laue−Langevin, Grenoble, France (Lindley et al., 1992). Sample−detector distances of 2.00 and 5.00 m were used. With the monochromator set for λ of 1.00 nm, and using a 64×64 cm^2 detector, the two detector settings resulted in a usable Q range of 0.06−1.1 nm^{-1}. When a rectangular beam aperture of 7×10 mm^2 was used, data acquisition times were typically 5 min in ^2H_2O buffers and 30 min in H_2O buffers. Samples were measured at 15 °C in rectangular quartz Hellma cuvettes of path length 2 mm for samples in ^2H_2O buffers and 1 mm for samples in H_2O buffers, and absorbances at 280 nm for AmiC concentrations were measured directly in the same cells. Sample and buffer transmissions were measured relative to an empty cell transmission for use in data reduction. Data were processed using standard Grenoble software (RNILS, SPOLLY, RGUIM, and RPLOT; Ghosh, 1989). A cadmium run for electronic and neutron background was first subtracted from each scattering curve. The buffer background run was subtracted from that of the sample run, and the result was normalized for the detector response by using a water run from which an empty cell background, corrected for the transmission of water, had been subtracted.

Neutron scattering data were also obtained in one session on the LOQ instrument at the pulsed neutron source ISIS at the Rutherford Appleton Laboratory, Didcot, U.K. (Heenan & King, 1993). The moderated pulsed neutron beam was derived from a tantalum target after proton bombardment at 50 Hz (proton beam current of 171 μA). Based on a fixed sample−detector distance of 4.3 m, the usable Q range was 0.1−2.0 nm^{-1}. The data acquisition time was 1 h at a sample temperaure of 15 °C. Other details of data collection and analyses are described elsewhere [e.g., Mayans et al. (1995) and Beavil et al. (1995)].

(c) Guinier and Distance Distribution Function Analyses of Reduced Scattering Data

In a given solute−solvent contrast, the radius of gyration R_G is a measure of structural elongation if the internal inhomogeneity of scattering densities has no effect. Guinier analyses at low Q give the R_G and the forward scattering at zero angle $I(0)$ (Glatter & Kratky, 1982):

$$\ln I(Q) = \ln I(0) - R_G^2 Q^2/3$$

This expression is valid in a QR_G range up to 1.5. The relative $I(0)/c$ values (c = sample concentration) for samples measured in the same buffer during a data session gives the relative molecular weights M_r of the proteins when referenced against a suitable standard (Kratky, 1963; Jacrot & Zaccai, 1981; Wignall & Bates, 1987). Data analyses employed an interactive graphics program SCTPL5 (A. S. Nealis, A. J. Beavil, and S. J. Perkins, unpublished software) on a Silicon Graphics 4D35S Workstation.

Indirect transformation of the scattering data in reciprocal space $I(Q)$ into that in real space $P(r)$ was carried out using GNOM (Svergun et al., 1988; Semenyuk & Svergun, 1991; Svergun, 1992).

$$P(r) = \frac{1}{2\pi^2}\int_0^\infty I(Q)Qr \sin(Qr)\, dQ$$

$P(r)$ corresponds to the distribution of distances r between volume elements. This offers an alternative calculation of R_G and $I(0)$ which is now based on the full scattering curve and also gives the maximum dimension L. For this, the X-ray $I(Q)$ curve in the range between 0.3 and 2.0 nm^{-1} contained 345 data points, which were reduced to 255 points by GNOM for the transformation. The LOQ neutron $I(Q)$ contained 76 data points in the Q range between 0.1 and 2.1 nm^{-1}. GNOM employs a regularization procedure with an automatic choice of the transformation parameter α to stabilize the $P(r)$ calculation (Svergun, 1992). The $P(r)$ curve contains 61 points. A range of maximum assumed dimensions D_{max} was tested, and the final choice of D_{max} was based on three criteria: (i) $P(r)$ should exhibit positive values; (ii) the R_G from GNOM should agree with the R_G from Guinier analyses; and (iii) the $P(r)$ curve should be stable as D_{max} is increased beyond the estimated macromolecular length.

(d) Automated Procedure for Debye Sphere Modeling of AmiC

The X-ray and neutron scattering curves were modeled using small single-density spheres to represent the AmiC structure. The X-ray and neutron scattering curve $I(Q)$ were calculated by an application of Debye's Law adapted to spheres of a single density (Perkins & Weiss, 1983):

$$\frac{I(Q)}{I(0)} = g(Q)\left(n^{-1} + 2n^{-2}\sum_{j=1}^{m} A_j \frac{\sin Qr_j}{Qr_j}\right)$$

$$g(Q) = (3(\sin QR - QR\cos QR))^2/Q^6R^6$$

where $g(Q)$ is the squared form factor for the sphere of radius R, n is the number of spheres filling the body, A_j is the number of distances r_j for that value of j, r_j is the distance between the spheres, and m is the number of different distances r_j. The method has been calibrated with known crystal coordinates (Smith et al., 1990; Perkins et al., 1993).

The monomeric AmiC−acetamide coordinates (Brookhaven PDB accession code: 1pea) formed the asymmetric unit in space group $P4_22_12$, and were used for all calculations. The coordinates were converted to spheres by placing all residue atoms within a three-dimensional grid of cubes of side 0.457 nm. A cube was included in the model if it contained sufficient atoms above a specified cutoff such that the total volume of the 580 cubes equaled that of the dry protein of 55.0 nm^3 calculated from the sequence (SWISSPROT name, AMIC_PEASE; accession code, P27017) (Chothia, 1975; Perkins, 1986). As AmiC contains 384 residues, while only 369 residues were visible in the crystal structure for reason of crystallographic disorder at the N- and C-termini, this procedure compensated for the 4% smaller volume present in the crystal structure. X-ray curve fits were based on a rescaled hydrated model, whose volume is the sum of the dry model and that of a hydration shell of 0.3 g of H_2O/g of AmiC. The latter corresponds to an electrostricted volume of 0.0245 nm^3 per bound H_2O (Perkins, 1986). The rescaled cube coordinates have sides of 0.496 nm and correspond to spheres of radius 0.308 nm. The sphere sizes are much less than the nominal resolution of $2\pi/Q_{max}$ of the scattering curves. No corrections were applied for X-ray wavelength spread or beam divergence as these are considered to be negligible. For both LOQ and D11 data, a 16% spread in λ for a nominal λ of 1.0 nm and a beam divergence of 0.016 radians were used to correct the calculated neutron scattering curve for the reasons discussed in Mayans et al. (1995). Neutron curve fits were used after X-ray curve fitting to confirm that possible solute−solvent contrast effects were not significant. The R_G value of the model was calculated from the Guinier fit of the calculated curve in the same Q range used for experimental data. The quality of the curve fit was defined using an R-factor $R_{2.0}$ to measure the agreement between the experimental and calculated X-ray curves in the Q range between 0.1 and 2.0 nm^{-1} (Smith et al., 1990; Beavil et al., 1995). For a given set of models and curve fits, the R_G and $R_{2.0}$ values were imported into a spreadsheet for filtering and sorting to identify the best fit. Models for oligomers were not retained if they contained less than 95% of the required total of spheres in order to exclude models with significant steric overlap between the monomers.

In application to the comparative simulations of Figure 1, two changes were made: (i) The Brookhaven database files themselves were used directly in the simulations without correction for residues not observed in the electron density maps. (ii) As only α-carbon coordinates were reported in the 2mbp structure, only the α-carbon coordinates in the 1omp structure were used for reason of consistency.

In application to automated X-ray curve-fitting analyses, INSIGHT II 95.0 (Biosym/MSI, San Diego, CA) was used for all manipulations. Three approaches were developed: (i) A symmetric trimer was considered by orientating arbitrarily three monomers parallel to each other along their long axes such that they were related by 120° rotations about a 3-fold Z-axis of symmetry. Starting from a model in which the centers of the three monomers were close to the central 3-fold axis of symmetry and the monomers were sterically overlapped, further models for curve calculations were generated using INSIGHT II macros by moving the monomers outward from the central Z-axis in 0.2 nm steps in a total range of 4 nm. (ii) Mixtures of monomeric, dimeric, trimeric, and tetrameric AmiC were considered by calculating the scattering curves for each of the crystallographic monomer, dimer, trimer, and tetramer. The putative dimer was generated using the symmetry-related transformation x, y, z to $y, x, -z$ by application of the crystallographic dyad at $x, x, {}^1/_2$ (Pearl et al., 1994). A putative tetramer was then

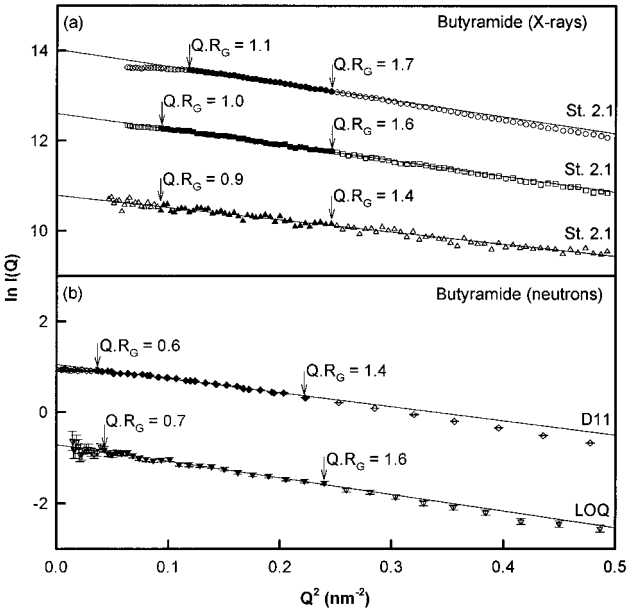

FIGURE 2: Guinier R_G plots for AmiC−butyramide. The filled symbols between the QR_G values as arrowed denote the range used to determine $I(0)$ and R_G. Statistical error bars are only shown when these are large enough to be visible. (a) Dilution series studied by synchrotron X-ray scattering for AmiC−butyramide at concentrations of 13.7 (○), 4.1 (□), and 1.0 mg/mL (△). The Q ranges for Guinier fits were 0.3−0.5 nm^{-1} for the 1 mg/mL curve and 0.35−0.5 nm^{-1} for the 13.7 mg/mL curve. (b) Neutron scattering data for AmiC−butyramide concentrations of 5.1 mg/mL used for D11 (◇) and 2.6 mg/mL used for LOQ (▽).

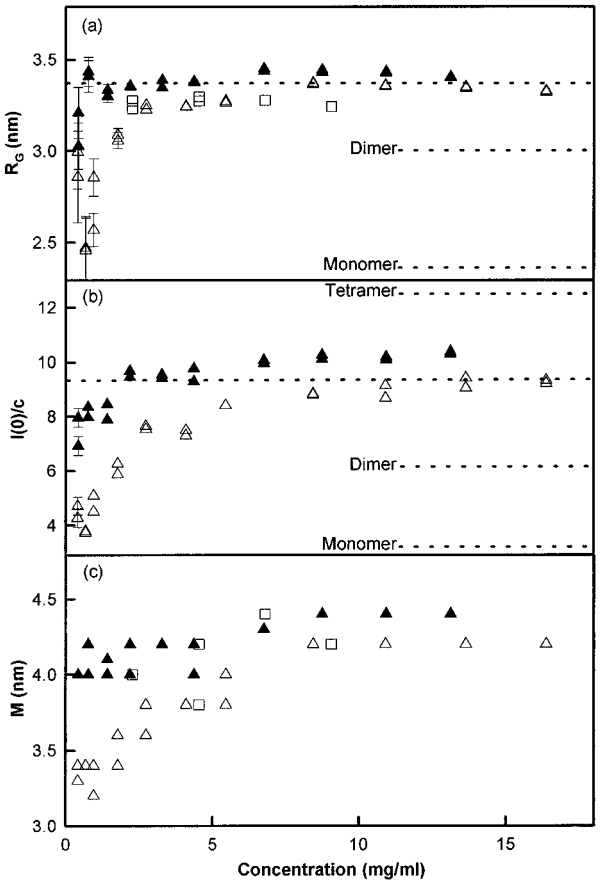

FIGURE 3: Concentration dependence of the AmiC X-ray Guinier and $P(r)$ parameters. Statistical error bars are only shown when these are large enough to be visible. (a) Those for the R_G values for AmiC−butyramide in two different beam-time sessions (□ and △) and for AmiC−acetamide (▲) is summarized. The dashed lines denote the R_G values of 1, 2, and 3 subunits of AmiC from Table 2 for comparison. (b) The corresponding $I(0)/c$ values for AmiC−butyramide and AmiC−acetamide are shown, using the same symbols as in a. The dashed lines denote the $I(0)/c$ values corresponding to the molecular weights for 1, 2, 3, and 4 subunits of AmiC. (c) The most frequently occurring distances M in $P(r)$ curves for AmiC−butyramide and AmiC−acetamide are shown, also using the same symbols as in a.

generated by application of the crystallographic dyad at $^1/_2$, $^1/_2$, z to this dimer. The putative trimer was formed by deleting any one of the four monomers in the tetramer. All combinations of these four curves in 1% steps were summed for fits with the experimental data. (iii) A putative asymmetric trimer model was considered using the crystallographic dimer and monomer. These were aligned manually so that their centers were close to each other without steric overlap. Cartesian axes were defined by reference to the center of mass of the AmiC monomer. The monomer was then moved −6 nm along its major translational Z-axis and −3 nm along the X- and Y-axes. The two structures were then translated in +0.2 nm steps relative to each other in the X, Y, and Z directions for distances of up to 12 nm using INSIGHT II macros, and the scattering curve was then calculated from each model for comparison with experimental data.

RESULTS AND DISCUSSION

(a) AmiC Oligomers by Synchrotron X-Ray Scattering

X-ray scattering data for AmiC in AmiC buffer containing 10 mM butyramide or 10 mM acetamide as appropriate (Methods) were obtained in the concentration range between 0.4 and 16.4 mg/mL. These are denoted as AmiC-buytramide and AmiC−acetamide respectively. Figure 2a shows that linear Guinier plots in satisfactory QR_G ranges were obtained. Guinier analyses of the 10 time frames used during data acquisition indicated the absence of radiation damage effects that are commonly seen with other proteins. However pronounced concentration effects were observed at above 10 mg/mL, where the Guinier plots exhibited diminished intensities at the lowest Q values. These are typical of interparticle interference effects when each protein molecule senses the presence of its neighbors (Guinier & Fournet, 1955). At these higher concentrations, a reduced QR_G range of fit corresponding to 0.35−0.5 nm^{-1} was required in order to obtain linear Guinier analyses.

The Guinier analyses showed that, at concentrations below 5 mg/mL, both the R_G and $I(0)/c$ values decreased with decrease in AmiC concentration (Figures 3a and 3b). This is typical of the dissociation of an oligomeric protein. The R_G and $I(0)/c$ values were consistently higher for AmiC−acetamide when compared with AmiC−butyramide, in particular at AmiC concentrations below 2 mg/mL, and again at above 10 mg/mL. This suggested that the presence of acetamide induced a higher degree of oligomer formation in AmiC compared to butyramide. In contrast, L-arabinose binding protein behaved as a monomeric protein in the concentration range 6−36 mg/mL of protein (Newcomer et al., 1981).

To determine whether a conformational change could be detected in AmiC when the ligand was changed from butyramide to acetamide, the R_G values for the two forms were compared for curves with identical $I(0)/c$ values (i.e., similar degrees of oligomerization). For an $I(0)/c$ value of

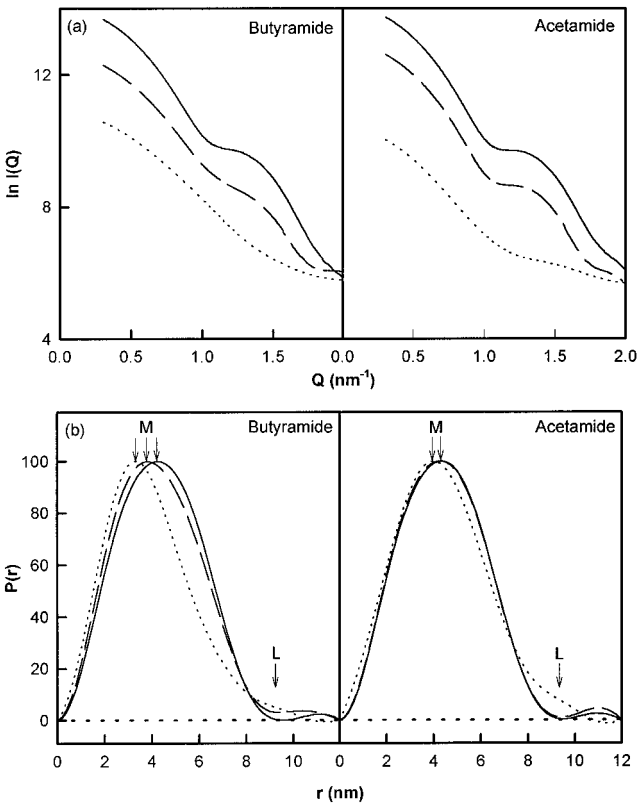

FIGURE 4: Comparison of the X-ray scattering curves $I(Q)$ and distance distribution functions $P(r)$ for AmiC−butyramide and AmiC−acetamide. (a) Concentration dependence of the X-ray $I(Q)$ curves for AmiC−butyramide and AmiC−acetamide. For clarity, the $I(Q)$ curves were smoothed using GNOM. Continuous, 13.7 mg/mL; dashed, 4.1 mg/mL; dotted, 1.0 mg/mL. (b) Corresponding distance distribution functions $P(r)$ for AmiC−butyramide and AmiC−acetamide. Each concentration is denoted as in a.

9.3, the full dashed lines in Figure 3a showed that the R_G values of AmiC−butyramide at 8−13 mg/mL were the same at 3.35 nm (within a range of 0.05 nm) to those for AmiC−acetamide at 3−5 mg/mL. This showed that no large conformational change had occurred within these limits. The errors in R_G values are larger at low concentrations, and it was not possible to consider this question for AmiC below 2 mg/mL. If the binding of acetamide had induced a rotational closure of the cleft in AmiC, the R_G value would be expected to be smaller by about 0.1 nm by analogy with L-arabinose binding protein (Newcomer et al., 1981).

Changes in AmiC oligomerization were also visible in the full scattering curves $I(Q)$ out to $Q = 2$ nm^{-1} (Figure 4a), in which a submaximum at Q of 1.2 nm^{-1} at high AmiC concentration disappeared at low AmiC concentration. Satisfactory distance distribution functions $P(r)$ were calculated from $I(Q)$ curves on the basis of a presumed maximum dimension D_{max} of 12 nm (Figure 4b). The $P(r)$ curves offered an alternative determination of R_G and $I(0)/c$, and these corroborated the Guinier analyses of Figures 3a and 3b (data not shown). The $P(r)$ curves also demonstrated a concentration dependence which is larger for AmiC−butyramide. At all concentrations, the maximum dimension L of AmiC is close to 9 nm and shows that the different oligomers are similar in overall length. The peak maximum M of the $P(r)$ curves corresponds to the most commonly occurring distance in AmiC. The concentration dependence of M in Figure 3c exhibited similar trends to those already observed with the R_G and $I(0)/c$ values, in that its position demonstrated a greater concentration dependence with AmiC−butyramide and ranged from 4.2 to 3.2 nm.

(b) Identification of AmiC Trimers by Neutron Scattering

Neutron scattering for AmiC in ^2H_2O buffers provided molecular weights as well as acting as a control for the absence of X-ray radiation damage effects and internal scattering density inhomogeneity effects in different solvents. AmiC is now visualized in a high negative solute−solvent contrast in place of the high positive contrast seen by X-rays. Linear Guinier R_G plots were obtained from both the neutron cameras D11 and LOQ (Figure 2b). The higher neutron flux on D11 permitted a dilution series of AmiC−butyramide and AmiC−acetamide to be measured between 0.8−5.1 mg/mL (data not shown). The neutron Guinier $I(0)/c$ values confirmed the X-ray concentration dependence in Figure 3b. The mean D11 R_G value for AmiC−butyramide was 3.26 ± 0.08 nm (five determinations between 1.2 and 5.1 mg/mL), and that for AmiC−acetamide was 3.30 ± 0.06 nm (four determinations between 0.8 and 1.9 mg/mL). The corresponding LOQ R_G values were in agreement at 3.30 ± 0.05 nm for AmiC−butyramide (one determination at 2.6 mg/mL) and 3.26 ± 0.06 nm for AmiC−acetamide (one determination at 2.8 mg/mL). The neutron R_G values were close to but slightly less than the X-ray value of 3.35 nm as expected (Table 2). The small decrease of up to 0.1 nm in the neutron R_G values is attributable to the surface location of hydrophilic amino acids and the core location of hydrophobic amino acids in AmiC, since hydrophilic residues have a higher scattering density than hydrophobic residues (Perkins, 1986, 1988).

M_r calculations were performed from the neutron $I(0)/c$ values, as $I(0)/c$ is measured relative to known standards. For D11 data, $I(0)/c$ for AmiC−butyramide at 3.9 mg/mL in H_2O buffer was determined to be 0.072 ± 0.005 relative to the incoherent scattering of H_2O at a wavelength of 1.0 nm, and this gave an M_r of 127 000 ± 10 000. Since monomeric AmiC has an M_r of 42 600, this is equivalent to 3.0 ± 0.2 subunits. For LOQ data, the mean $I(0)/c$ value of 0.176 observed for AmiC−butyramide and AmiC−acetamide referenced to a known polymer standard and other $I(0)/c$ values determined for five proteins of known M_r between 51 000 and 144 000 (Mayans et al., 1995; Ashton et al., 1995; Beavil et al., 1995) gave an M_r of 150 000 ± 25 000, which corresponds to 3.6 ± 0.6 subunits. The full X-ray $I(0)/c$ concentration series in Figure 3b shows that AmiC is predominantly trimeric between 5 and 10 mg/mL and undergoes significant dissociation at concentrations below 5 mg/mL. As an $I(0)/c$ value of 9.3 can be assigned to 3 AmiC subunits in Figure 3b, an $I(0)/c$ value of 3.1 will correspond to monomeric AmiC. Figure 3a shows that the R_G of the AmiC monomer is less than 2.5 nm and that AmiC dissociates into monomers at low concentrations.

(c) X-ray Scattering Curve Simulations for Three Periplasmic Binding Proteins

Curve simulations were performed using known crystal structures for free and complexed forms of the periplasmic binding proteins in order to assess whether solution scattering will monitor domain movements between their open and closed conformations.

(i) The periplasmic binding proteins from six clusters (Tam & Saier, 1993) exhibited R_G values between 1.99 and 2.56

Table 2: X-ray and Neutron Scattering Parameters for AmiC Samples and Models

technique (instrument)	protein	concentration (mg/mL)	experimental R_G (nm)
synchrotron X-ray (St 2.1)	AmiC−butyramide	7−16	3.35 ± 0.05
	AmiC−acetamide[a]	2−5	3.35 ± 0.05
	AmiC−acetamide[a]	0.4	3.12 ± 0.13
neutron (D11)	AmiC−butyramide	1.2−5.1	3.26 ± 0.08
	AmiC−acetamide[a]	0.8−1.9	3.30 ± 0.06
neutron (LOQ)	AmiC−butyramide	2.6	3.30 ± 0.05
	AmiC−acetamide[a]	2.8	3.26 ± 0.06

AmiC models	concentration (mg/mL)	*R* factor (2.0 nm^{-1})	modeled R_G (nm)
AmiC scattering (symmetric trimer)	6.8[b]	4.7	3.39
AmiC crystallographic monomer			2.34
AmiC crystallographic dimer			2.97
AmiC crystallographic trimer[c]			3.53
AmiC crystallographic tetramer			3.66
AmiC scattering (dimer + tetramer)	6.8[b]	6.3	3.38
AmiC scattering (asymmetric trimer 1)	6.8[b]	4.1	3.34
AmiC scattering (asymmetric trimer 2)	6.8[b]	3.9	3.32

[a] Not shown in Figure 2. [b] Shown in Figures 5 and 6. [c] Generated by deleting any one of the four AmiC structures in the tetramer.

nm in an M_r range between 26 100 and 59 100 (Table 1). The Cluster 4 proteins AmiC and LivJ showed a decrease of 0.21 nm in R_G values on going from the unbound to the complexed form. The Cluster 3 proteins gave a smaller decrease of 0.13 nm, and that for the Cluster 1 proteins gave a decrease of 0.08 nm (Table 1).

(ii) Corresponding changes were seen in the full scattering curves out to Q of 2.0 nm^{-1} for these three groups of proteins (Figure 1). The scattering curve at low Q exhibited small changes which corresponded to the changes in the Guinier region. More noticeable intensity changes between the free and complexed forms were visible in the Q range beyond 1 nm^{-1}.

Figure 1 also indicates the domain movements between the free and complexed forms of these proteins when the C-terminal domains were superimposed upon each other. While large domain movements of the order of 30−40° are observed and are detectable by solution scattering, Figure 1 and Table 1 show that accurate measurements will be required. In the case of trimeric AmiC, no domain movements could be detected within a precision in R_G values of 0.05 nm.

(d) X-ray Scattering Curve Simulations for Trimeric AmiC

To extend the data interpretation, scattering curve simulations were performed in three different analyses for trimeric AmiC, starting from the crystal structure for AmiC−acetamide. The trimer will have a 3-fold axis of symmetry, as observed crystallographically for proteins such as tumor necrosis factor α, deoxyUTPase, and chloramphenicol transferase. A structure based on the asymmetric association of a monomer with a dimer is most unlikely on the grounds of symmetry. If a monomer is bound to one face of a dimer in such a trimer, a symmetry-related site for a second monomer will exist on the other side of the dimer, and AmiC would be tetrameric.

A symmetric AmiC homotrimer was constructed from three monomers whose longest axes were aligned parallel to each other with their ligand clefts arbitrarily set to face outward and with a 3-fold axis of symmetry between them along the *Z*-axis (Figure 5). Based on the scattering curve for AmiC−butyramide at 6.8 mg/mL, a one-parameter translational search explored the effect of varying the separation between the monomers in the *XY*-plane while retaining 3-fold symmetry. The best model by this approach in Figure 5 gave a good curve fit, 3s in Figure 6, with a low $R_{2.0}$ value of 4.7%. This model also resulted in a good fit (not shown) to the experimental curve at 1 mg/mL in Figure 4a with a satisfactory $R_{2.0}$ value of 7.3%, using a scattering curve constructed from 40% monomer and 60% homotrimer (curves 1 and 3s in Figure 6). This monomer:trimer ratio resulted in an estimated association constant K_{a3} of 2×10^{10} M^{-2}, where $K_{a3} = c_{trimer}/(c_{monomer})^3$ (McRorie & Voelker, 1993).

A second analysis was based on the monomer in the crystal structure of AmiC−acetamide, together with the putative dimer, trimer, and tetramer (curves 1, 2, 3, and 4, respectively, in Figure 6: see Materials and Methods). The curves changed in the Q range between 0.0 and 0.5 nm^{-1} to correspond to the increase in R_G with oligomerization (Table 2). The dimer model (Figure 5) gave a reasonable curve fit for AmiC−butyramide at 1.0 mg/mL with an $R_{2.0}$ value of 8.0%, but this fit was visibly not as good as that for the monomer−homotrimer mixture above. In terms of the AmiC−butyramide scattering curve at 6.8 mg/mL, the four models gave poor curve fits with $R_{2.0}$ values of 15.3%, 12.1%, 9.7%, and 39.3%, respectively. In particular, the experimental curve at 6.8 mg/mL showed a subminimum at $Q = 1.12$ nm^{-1}, which is different from that at $Q = 0.98$ nm^{-1} calculated from the tetramer model (curve 4). It was postulated that the observed curve may represent a combination of the four curves. Analysis of 5151 combinations of any three curves stepped in 1% increments gave a best fit with 0% monomer, 51% dimer, and 49% tetramer. Analysis of all 176 851 combinations of four curves gave a best fit with 0% monomer, 51% dimer, 0% trimer, and 49% tetramer (curves 2 and 4 in Figure 6). Although the $R_{2.0}$ value of 6.3% for this fit is reasonable, the curve fit is seen to deviate at Q values above 0.8 nm^{-1}. The limited success of these fits showed that the putative tetramer does not exist, and this supports the modeling based on a monomer−trimer equilibrium.

A third curve fit search assumed that AmiC at 6.8 mg/mL corresponded to an asymmetric trimer formed from the crystallographic monomer and dimer. In three-parameter *X*-,

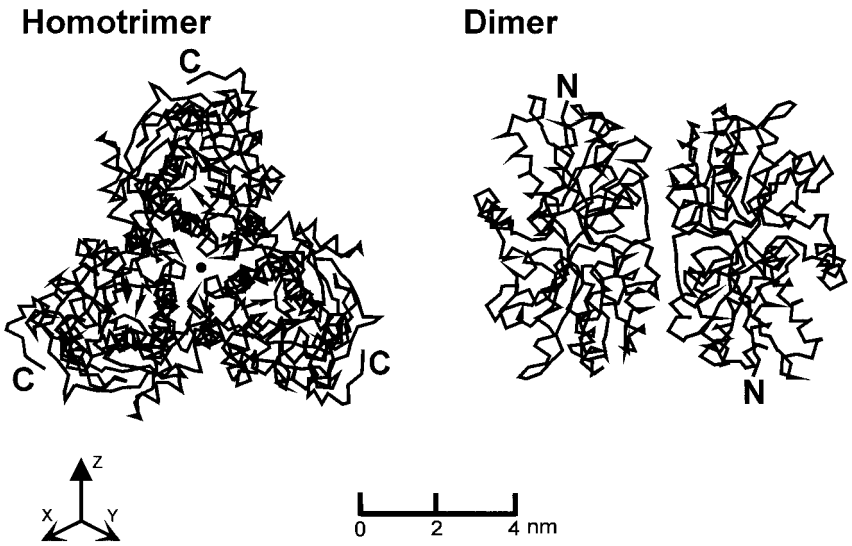

FIGURE 5: α-Carbon outlines of the homotrimer and dimer models for AmiC, based on the AmiC−acetamide crystal structure. The homotrimer of AmiC is viewed down the *Z*-axis which is indicated by the dot at the center of the structure. The C-termini in this model are denoted by C. In the final model, the center of mass of the monomer is 2.2 nm from the center of mass of the trimer on its 3-fold axis of symmetry. The putative crystallographic dimer is depicted as an antiparallel association of two monomers, in which the N-termini are denoted by N. In the putative crystallographic tetramer, the second dimer is rotated clockwise by 135° which is then positioned in front of the first dimer as shown.

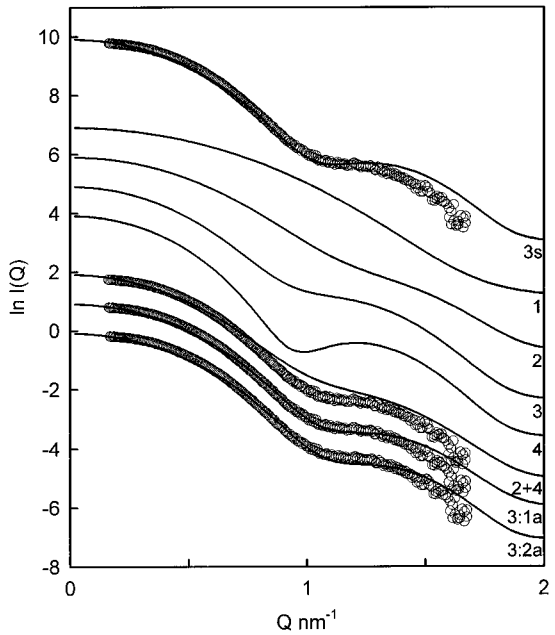

FIGURE 6: Curve fits of experimental scattering curves for AmiC−butyramide. Symmetric homotrimer, 3s; monomer, 1; dimer, 2; trimer, 3; tetramer, 4; asymmetric trimers, 3:1a and 3:2a (Table 2). The curves were compared with X-ray data for AmiC−butyramide at 6.8 mg/mL. The asymmetric trimer 1 corresponds to an AmiC monomer with its long axis perpendicular to that of the dimer (Figure 5). The monomer coordinates are superimposed on one of the two monomers in the dimer by translations of $X = 1.7$ nm, $Y = 2.7$ nm, $Z = -1.5$ nm and rotations of $X = 95°$, $Y = 12°$, $Z = -90°$. Trimer 2 was generated from a 90° reorientation of the AmiC monomer such that the long axes of the monomer and dimer are parallel. The monomer coordinates are superimposed on one of the two monomers in the dimer by translations of $X = -0.02$ nm, $Y = -3.0$ nm, $Z = -2.0$ nm and rotations of $X = -14°$, $Y = -20°$, $Z = 195°$.

Y-, and *Z*-axis translational searches, the long axis of the monomer was set perpendicular (curve 3:1a) or parallel (curve 3:2a) to that of the dimer. A clear minimum in the $R_{2.0}$ values was obtained for each of the *X*-, *Y*-, and *Z*-axes in trial translational searches and showed that a global minimum could be defined. The full systematic search was based on 31 × 31 × 41 steps of 0.2 nm along the *X*-, *Y*-, and *Z*-axes and gave 39 401 coordinate models. Models were selected if they contained at least 1650 of the expected total of 1752 spheres (i.e., only those models without monomer−dimer steric overlap were retained) and had a calculated R_G value between 3.0 and 3.5 nm. From these searches, the best curve fits, 3:1a and 3:2a, had similar $R_{2.0}$ values of 3.9% and 4.1%, respectively (Figure 6 and Table 2). While these $R_{2.0}$ values are now better than those above, the importance of this search is that it showed that a good fit can be obtained from a model with incorrect symmetry. As these models gave the best fits, they were also used for neutron curve fits as a check of consistency. The fits (not shown) gave good *R* factors in both H_2O and ^2H_2O buffers, and the calculated curve deviated slightly from the two observed curves in opposite directions at larger *Q* values as expected from the two opposite solute−solvent contrasts in use.

CONCLUSIONS

The classical view of periplasmic binding proteins is that they are monomeric with two domains that undergo large conformational change during ligand binding. While AmiC is most closely related to the Cluster 4 protein LivJ in sequence and structure, AmiC is a cytoplasmic protein that controls the activity of AmiR which is directly involved with *ami* gene expression, while LivJ is a perisplasmic protein that binds aliphatic amino acids. Both exhibit similar interactions with membrane-bound proteins (Wilson et al., 1995). Unexpectedly AmiC exhibits oligomeric properties at high concentrations. Other periplasmic binding proteins are generally monomeric, although the galactose binding protein from *Salmonella typhimurium* and *E. coli* and the maltose binding protein from *E. coli* are dimeric, and the addition of ligand causes them to become monomeric (Mowbray & Petsko, 1983; Richarme, 1982). The crystal structures of histidine-binding protein (1hsl) and a maltodextrin-binding protein mutant (1mdp) reveal dimeric struc-

tures; however, these are attributable to repeated lattice contacts between the same domain in a pair of monomers. In distinction to these examples, AmiC forms antiparallel dimers in its crystal structure (Figure 5), most probably the consequence of the crystal lattice, and it participates in a monomer−trimer association in solution. These results show that AmiC behaves differently from the classical periplasmic binding proteins.

Above 2 mg/mL, AmiC is predominantly trimeric. That trimer formation is promoted in the presence of its ligand acetamide rather than the anti-inducer butyramide may be of biological interest. The concentration dependence of the scattering curves is clear from Figure 4, and the $I(0)/c$ graphs rise with c to a value corresponding to trimers in Figure 3. Initial analytical ultracentrifugation data by sedimentation equilibrium methods using a Beckman XLA ultracentrifuge also showed this concentration dependence and yielded a comparable estimate of the association constant K_{a3} (O. Byron, D. Chamberlain, and S. J. Perkins, unpublished data; Ralston, 1993; McRorie & Voelker, 1993). Molecular modeling based on the AmiC−acetamide crystal structure showed that trimeric structures gave R_G values that corresponded to the observed values. The possibility of an imposter model based on a mixture of dimers and tetramers was also considered. This was discounted for two reasons: (i) A single peak and not a double peak was routinely observed during AmiC purifications by gel filtration (Methods). (ii) Modeling of the X-ray data showed that it was not possible to optimize a curve fit based on a mixture of dimer and tetramer that was equivalent to or better than one based on a trimer (Figure 6).

Unlike periplasmic binding proteins in general, scattering showed that no conformational changes between AmiC−acetamide and AmiC−butyramide trimers could be detected within a precision of 0.05 nm in R_G value. Butyramide contains an extra pair of CH_2•CH_2 carbon atoms. As butyramide binds 100-fold more weakly to AmiC than acetamide (Wilson et al., 1993), this weaker binding may reflect the energy required to accommodate butyramide within its binding site in AmiC without a large cleft opening. Trimer formation in AmiC would involve extensive contacts between the monomers and may hinder the free movement of the cleft on change of ligand. The question of whether this domain movement occurs or not on ligand binding will require data collection on monomeric AmiC or on the complex between AmiC and AmiR. Nonetheless the larger size of the butyramide ligand has clearly reduced the stability of the AmiC trimer.

Solution scattering will monitor domain movements in the periplasmic binding proteins, even though the changes are small (Figure 1 and Table 1). Here, even though L-arabinose binding protein was monomeric and well-behaved between concentrations of 4 and 36 mg/mL (Newcomer *et al.*, 1981), AmiC demonstrated interparticle interference effects above 10 mg/mL as well as oligomer formation in its scattering curves. Dilution series and absolute M_r calculations were key controls of the present scattering data. Data analyses were enhanced by the use of automated constrained curve fitting procedures. Hypotheses could be stated which could then be tested in detail with relatively little effort, although expensive in terms of CPU time, and enabled a choice to be made between a monomer−trimer or a monomer−dimer−tetramer association. Automated curve fits had previously been used to assess domain structures in single large multidomain proteins (Mayans et al., 1995; Beavil et al., 1995; Boehm et al., 1996). The present study shows that the method is applicable to the study of protein−protein complexes. It should be noted that a good curve fit is only a test of consistency and will not constitute a unique low-resolution structure determination. The good curve fit obtained for the symmetry-forbidden asymmetric trimer of AmiC is an illustration of this limitation.

Following the scattering studies, thermal denaturation experiments (B. P. O'Hara, G. Siligardi, S. A. Wilson, R. E. Drew, and L. H. Pearl, 1997, manuscript in preparation) have shown that AmiC−butyramide is less stable than AmiC−acetamide. The crystal structure of AmiC−butyramide has been determined and shows that no major conformational changes in AmiC were observed. The root mean square difference between the α-carbon coordinates of both forms of AmiC was 0.040 nm. This is supported by circular dichroism spectroscopy of AmiC−butyramide and AmiC−acetamide which also suggested no major conformational changes. These results are consistent with the present scattering data.

ACKNOWLEDGMENT

We thank the Biotechnology and Biological Sciences Research Council for an Earmarked studentship to D.C. and for grant support. We thank Dr. R. E. Drew for useful discussions, Mr. A. W. Ashton for computational support, the Engineering and Physical Sciences Research Council for X-ray and neutron facilities, and Dr. E. Towns-Andrews, Mrs. S. Slawson, Mr. A. Gleeson, Dr. P. A. Timmins, Dr. R. K. Heenan, and Dr. S. M. King for generous instrumental support.

REFERENCES

Ashton, A. W., Kemball-Cook, G., Johnson, D. J. D., Martin, D. M. A., O'Brien, D. P., Tuddenham, E. D. G., & Perkins, S. J. (1995) *FEBS Lett. 374*, 141−146.

Beavil, A. J., Young, R. J., Sutton, B. J., & Perkins, S. J. (1995) *Biochemistry 34*, 14449−14461.

Boehm, M. K., Mayans, M. O., Thornton, J. D., Begent, R. H. J., Keep, P. A., & Perkins, S. J. (1996) *J. Mol. Biol. 259*, 718−736.

Chothia, C. (1975) *Nature (London) 254*, 304−308.

Drew, R. E., & Wilson, S. A. (1992) in *Pseudomonas: Molecular Biology and Biotechnology* (Galli, E., Silver, S., & Witholt, E., Eds) pp 207−213, American Society of Microbiology, Washington, DC.

Ghosh, R. E. (1989) Institut Laue-Langevin Internal Publication No. 89GH02T, Institut Laue-Langevin, Grenoble, France.

Glatter, O., & Kratky, O., Eds. (1982) *Small-Angle X-ray Scattering*, Academic Press, New York.

Guinier, A., & Fournet, G. (1955) *Small Angle Scattering of X-rays*, Wiley, New York.

Heenan, R. K., & King, S. M. (1993) Proceedings of an International Seminar on Structural Investigations at Pulsed Neutron Sources, Dubna, Russia, September 1−4, 1992, Report E3-93-65, Joint Institute for Nuclear Research, Dubna, Russia.

Heenan, R. K., King, S. M., Osborn, R., & Stanley, H. B. (1989) Colette Users Guide, Internal Publication No. RAL-89-128, Rutherford Appleton Laboratory, Didcot, U.K.

Jacrot, B., & Zaccai, G. (1981) *Biopolymers 20*, 2413−2426.

Jawetz, E., Melnick, J. L., & Adelberg, E. A. (1987) *Review of Medical Microbiology*, 17th ed., Appleton & Lange, Norwalk, CT.

Kelly, M., & Clarke, P. H. (1962) *J. Gen. Microbiol. 27*, 305−316.

Koch, C., & Høiby, N. (1993) *Lancet 341*, 1065−1069.

Kratky, O. (1963) *Progr. Biophys. Chem. 13*, 105−173.
Lindley, P., May, R. P., & Timmins, P. A. (1992) *Physica B 180*, 967−972.
Luecke, H., & Quiocho, F. A. (1990) *Nature (London) 347*, 402−406.
Mayans, M. O., Coadwell, W. J., Beale, D., Symons, D. B. A., & Perkins, S. J. (1995) *Biochem. J. 311*, 283−291.
McRorie, D. K., & Voelker, P. J. (1993) *Self-Associating Systems in the Analytical Ultracentrifuge*, Beckman Instruments Inc., Fullerton, CA.
Mowbray, S. L., & Petsko, G. A. (1983) *J. Biol. Chem. 258*, 7991−7997.
Newcomer, M. E., Lewis, B. A., & Quiocho, F. A. (1981) *J. Biol. Chem. 256*, 13218−13222.
Oh, B.-H., Pandit, J., Kang, C.-H., Nikaido, K., Gokcen, S., Ames, G. F.-L., & Kim, S.-H. (1993) *J. Biol. Chem. 268*, 11348−11355.
Oh, B.-H., Kang, C.-H., De Bondt, H., Kim, S.-H., Nikaido, K., Joshi, A. K., & Ames, G. F.-L. (1994) *J. Biol. Chem. 269*, 4135−4143.
O'Hara, P. J., Sheppard, P. O., Thøgersen, H., Venezia, D., Haldeman, B. A., McGrane, V., Houamed, K. M., Thomsen, C., Gilbert, T. L., & Mulvihill, E. R. (1993) *Neuron 11*, 41−52.
Pearl, L. H., O'Hara, B., Drew, R. E., & Wilson, S. A. (1994) *EMBO J. 13*, 5810−5817.
Perkins, S. J. (1986) *Eur. J. Biochem. 157*, 169−180.
Perkins, S. J. (1988) in *New Comprehensive Biochemistry* (Neuberger, A., & Van Deenen, L. L. M., Eds.) Vol. 11B, Part 2, pp 143−264, Elsevier, Amsterdam.
Perkins, S. J., & Weiss, H. (1983) *J. Mol. Biol. 168*, 847−866.
Perkins, S. J., Smith, K. F., Kilpatrick, J. M., Volanakis, J. E., & Sim, R. B. (1993) *Biochem. J. 295*, 87−99.
Pflugrath, J. W., & Quiocho, F. A. (1988) *J. Mol. Biol. 200*, 163−180.
Quiocho, F. A., Wilson, D. K., & Vyas, N. K. (1989) *Nature (London) 340*, 404−407.
Ralston, G. (1993) *Introduction to Analytical Ultracentrifugation*, Beckman Instruments Inc., Fullerton, CA.
Richarme, G. (1982) *Biochem. Biophys. Res. Commun. 105*, 476−481.
Sack, J. S., Saper, M. A., & Quiocho, F. A. (1989a) *J. Mol. Biol. 206*, 171−191.
Sack, J. S., Trakhanov, S. D., Tsigannik, I. H., & Quiocho, F. A. (1989b) *J. Mol. Biol. 206*, 193−207.
Semenyuk, A. V., & Svergun, D. I. (1991) *J. Appl. Crystallogr. 24*, 537−540.
Sharff, A. J., Rodseth, L. E., Spurlino, J. C., & Quiocho, F. A. (1992) *Biochemistry 31*, 10657−10663.
Singleton, P., & Sainsbury, D. (1987) *Dictionary of Microbiology and Molecular Biology*, 2nd ed., pp 719−720, Wiley, Chichester, U.K.
Smith, K. F., Harrison, R. A., & Perkins, S. J. (1990) *Biochem. J. 267*, 203−212.
Spurlino, J. C., Lu, G.-Y., & Quiocho, F. A. (1991) *J. Biol. Chem. 266*, 5202−5219.
Stanier, R. Y., Palleroni, N. J., & Doudoroff, M. (1966) *J. Gen. Microbiol. 43*, 159−271.
Stern-Bach, Y., Bettler, B., Hartley, M., Sheppard, P. O., O'Hara, P. J., & Heinemann, S. F. (1994) *Neuron 13*, 1345−1357.
Svergun, D. I. (1992) *J. Appl. Crystallogr. 25*, 495−503.
Svergun, D. I., Semenyuk, A. V., & Feigin, L. A. (1988) *Acta Crystallogr. A44*, 244−250.
Tam, R., & Saier, M. H., Jr. (1993) *Microbiol. Rev. 57*, 320−346.
Tame, J. R. H., Murshudov, G. N., Dodson, E. J., Neil, T. K., Dodson, G. G., Higgins, C. F., & Wilkinson, A. J. (1994) *Science 264*, 1578−1581.
Towns-Andrews, E., Berry, A., Bordas, J., Mant, G. R., Murray, P. K., Roberts, K., Sumner, I., Worgan, J. S., Lewis, R., & Gabriel, A. (1989) *Rev. Sci. Instrum. 60*, 2346−2349.
Wignall, G. D., & Bates, F. S. (1987) *J. Appl. Crystallogr. 20*, 28−40.
Wilson, S. A., & Drew, R. E. (1991) *J. Bacteriol. 173*, 4914−4921.
Wilson, S. A., Chayen, N. E., Hemmings, A. M., Drew, R. E., & Pearl, L. H. (1991) *J. Mol. Biol. 222*, 869−871.
Wilson, S. A., Wachira, S. J., Drew, R. E., Jones, D., & Pearl, L. H. (1993) *EMBO J. 12*, 3637−3642.
Wilson, S. A., Williams, R. J., Pearl, L. H., & Drew, R. E. (1995) *J. Biol. Chem. 270*, 18818−18824.
Worgan, J. S., Lewis, R., Fore, N. S., Sumner, I. L., Berry, A., Parker, B., D'Annunzio, F., Martin-Fernandez, M. L., Towns-Andrews, E., Harries, J. E., Mant, G. R., Diakun, G. P., & Bordas, J. (1990) *Nucl. Instrum. Methods Phys. Res. A291*, 447−454.
Yao, N., Trakhanov, S., & Quiocho, F. A. (1994) *Biochemistry 33*, 4769−4779.

BI9703251